Metal Substitution as the Method of Modifying Electronic Structure of Metal−Organic Frameworks

Maria A. Syzgantseva,[†] Christopher Patrick Ireland,[‡] Fatmah Mish Ebrahim,[‡] Berend Smit,[‡] and Olga A. Syzgantseva*,[‡]

[†]Laboratory of Quantum Mechanics and Molecular Structure, Department of Chemistry, Moscow State University M.V. Lomonosov, Moscow 119991, Russia

[‡]Laboratory of Molecular Simulation (LSMO), Institut des Sciences et Ingénierie Chimiques, Valais Ecole Polytechnique Fédérale de Lausanne (EPFL), Rue de l'Industrie 17, CH-1951 Sion, Switzerland

Ⓢ *Supporting Information*

ABSTRACT: Targeted modification of electronic structure is an important step in the optimization of metal−organic frameworks (MOFs) for photovoltaic, sensing, and photo-catalytic applications. The key parameters to be controlled include the band gap, the absolute energy position of band edges, the excited state charge separation, and degree of hybridization between metal and ligand sites. Partial metal replacement, or metal doping, within secondary building units is a promising, yet relatively unexplored route to modulate these properties in MOFs. Therefore, in the present study, a general method for selecting metal dopant is worked out in theory and validated by experiment, retaining MIL-125 and UiO-66 as the model systems. Metal mixing enables targeted optimization of key electronic structure parameters. This method is applicable to any MOF architecture and can serve as a roadmap for future synthesis of MOFs with predefined properties.
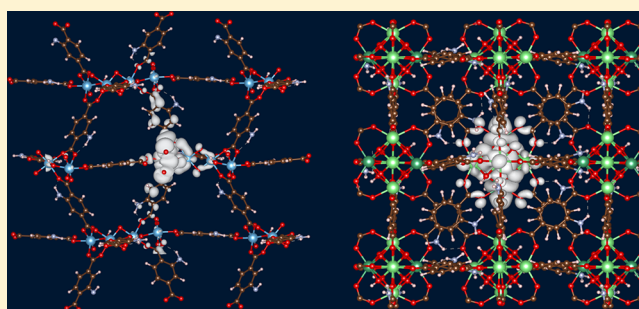
INTRODUCTION

Metal−organic frameworks (MOFs) have the promise that by changing the building blocks, the organic ligands, and metal nodes,[1,2] we can design an optimal material for an increasing range of applications.[3] Their unique chemical tunability offers the potential to decisively change the field: instead of relying on traditional methods of trial and error, we now have the quantum chemistry at hand to tailor-make materials. Yet, lack of theoretical studies restricts the number of compounds we can synthesize, characterize, and fully test for any of these applications. These limitations have motivated theoretical investigations[4,5] to support the experimental efforts. While the focus of most of these computational studies has been on finding the optimal materials for gas separation or storage,[6−13] far less theoretical work has been directed toward the emerging applications of MOFs, such as photovoltaics, sensing, and photocatalysis.[14−18] These applications are interesting from a computational point of view, as they require a detailed understanding of the principles governing MOF band structure modulation.

Key electronic structure characteristics to be optimized for efficient photoinduced applications comprise band gap, valence and conduction band edge energy alignment, excited state ligand−metal charge separation, and charge carrier lifetimes (Figure 1).

Precisely, a MOF should have an optimal band gap, preferentially tuned to a wavelength domain at which one
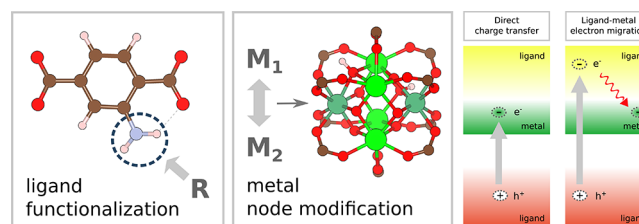
Figure 1. Strategies for compositional tuning of MOF photoactivity by ligand functionalization (changing side group R) or metal node modification (replacing metal $M_1^{n_1+}$ with $M_2^{n_2+}$). Excited state pathways to achieve a metal node reduction in a MOF.

would like the light absorption to take place. To enable an efficient charge transfer at the heterojunction or from/toward the substrate, the position of valence and conduction band edges should be energetically favorable. Upon creation of an electron−hole pair, an efficient electron migration toward an active site or an interface is essential. Besides, in the particular case of redox catalysis, one would like to ensure that the active centers are traps of the electrons and holes. In addition, the excited charge carrier lifetime needs to be sufficiently long to avoid the recombination before the injection at the interface or transfer toward a substrate takes place.

To solve these challenges, a lot of effort is put into finding an optimal metal−ligand combination that combines all these properties. However, one can also envision a strategy in which one tries to further improve the performance of an existing MOF. One attractive strategy is the partial replacement of metals within the nodes, creating mixed-metal MOFs. This is a synthetically achievable approach, as some examples of such mixed-metal systems are already known.[19−29] Practically, partial metal replacement allows *modifying the absolute and relative energy position of metal states* within the band structure of a MOF. Therefore, it is important to provide a roadmap for the selection of these dopants to engineer the electronic structure of existing compounds or new MOFs.

As model systems, we select MIL-125(Ti)-NH$_2$ and UiO-66(Zr)-NH$_2$ (Figure 2), both of which have a similar optical
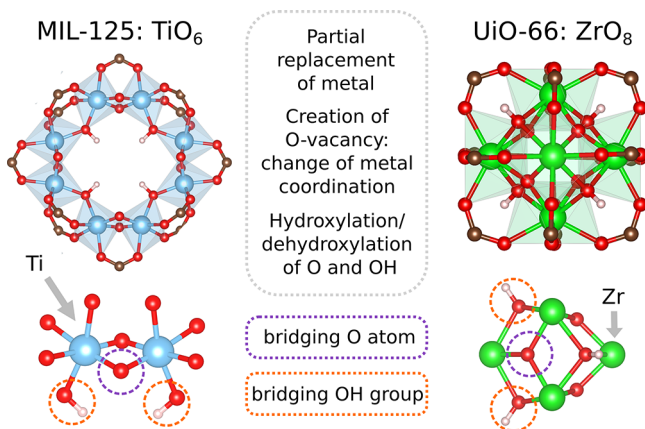
**Figure 2.** Structures of metal nodes in MIL-125 and UiO-66 architectures.

absorption spectrum with onset in the visible region[30,31] and are considered for usage in photocatalysis and photovoltaics.[14,32−34] In a combined experimental and computational study we show how doping with V and Nb in MIL-125 and UiO-66 allows us to tune the optical properties.

■ TOWARD A DOPING STRATEGY

As discussed in the previous section, the doping of metal nodes in a MOF can allow shifting metal states with respect to the electronic levels of the host. Deciding on which metal to use, it is important to recall that the position of its states is defined, among others, by the *electron affinity* of a metal node. Thus, choosing, for example, a metal with a higher electron affinity would enable placing its states below the ligand levels in the conduction band.

As metal nodes in a MOF can be often seen as embedded metal oxide clusters, one can apply the reducibility criteria of metal oxides to select an appropriate dopant. For MOFs the most appropriate criteria are a sufficiently small band gap and a high electron affinity (Figure 3), as defined by the absolute position of the conduction band edge.[35,36]

The amplitude of this electron level modulation depends on the concentration of dopant, which is another leverage for band structure tuning. The choice of a concentration should be facilitated by modeling doped MOF band structure in a different concentration range. To apply these general considerations to specific examples, we explore shifting metal states in the conduction band in MIL-125-NH$_2$(Ti) and UiO-66-NH$_2$(Zr) (see Figure 3). The potential dopants are nd^0
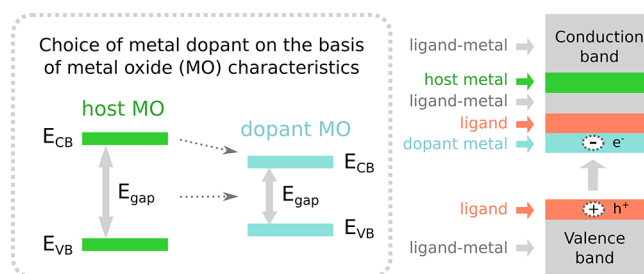
Figure 3. Modification of band gap, conduction band alignment, and creation of localized electron traps using metal doping of a MOF.

transition or main group metals, in their highest oxidation state (e.g, V, Sn, W, Ta, Nb). Using the extensive literature on oxides, we can further refine the selection set to ensure that within the oxide state band positions align well.[35,36]

In terms of absolute position, V_2O_5, SnO_2, WO_3, Ta_2O_5, and Nb_2O_5 conduction bands are situated lower in energy, as compared to both titania and zirconia.[35] Their band gaps are smaller than that of ZrO_2, while only Ta_2O_5, SnO_2, and Nb_2O_5 have larger band gaps than TiO_2.[35] Despite the fact that compared to ZrO_2 most of the above oxides have a higher electron affinity, not all of them necessarily are interesting dopants for UiO-66. Those having a larger electron affinity difference with ZrO_2 will merely create deep trap states instead of shallow ones, shifting the lowest unoccupied crystal orbital (LUCO) state below the thermodynamic limit for a possible reduction reaction and facilitating undesirable defect-induced nonradiative electron−hole recombination.

Hence, according to these criteria it is interesting to investigate Ti replacement in MIL-125-NH$_2$ by V, Sn, W, and Nb and Zr replacement in UiO-66-NH$_2$ by Ta, Nb, W, and Ti.[35,36] In addition, we consider Y for Zr replacement, as Y_2O_3 has a similar band gap to ZrO_2, although its conduction band edge is higher. Besides, as Ti doping of UiO-66 was already extensively studied,[27,37] it is not considered here. Due to the differences between the electronic structure of MOFs and metal oxides imposed by the presence of ligands and finite size of metal oxide clusters in their structure, the accurate effect of dopant, preselected following this procedure, requires accurate electronic structure calculations of the corresponding MOF, to make a final selection.

For this purpose, we compute the density of states, evaluate absolute energy positions of band edges, and analyze LUCOs in doped MIL-125-NH$_2$ and UiO-66-NH$_2$. This study is performed within the density functional theory, using the HSE06 functional[38] for electronic structure calculations to ensure accurate description of band gaps and conduction band (CB) positions of main group and transition metals. A detailed description of computational methods is given in the Supporting Information (SI).

Considering MIL-125-NH$_2$, its doping is supposed to enhance the localization on metal states, reducing the contribution of the ligand. As demonstrated below, Sn, W, V, and Nb have various effects on its electronic structure.

Introduction of V into MIL-125-NH$_2$ leads to a remarkable localization effect both in space and among chemical species (localization on V atoms), substantially reducing the contribution of the organic part as compared to pure MIL-125-NH$_2$ (Figure 4). Indeed, a total amount of LUCO electron density localized on metals is 0.46 e$^-$ in pristine MIL-125-NH$_2$ versus 0.73 e$^-$ in its V-doped counterpart with 1/8
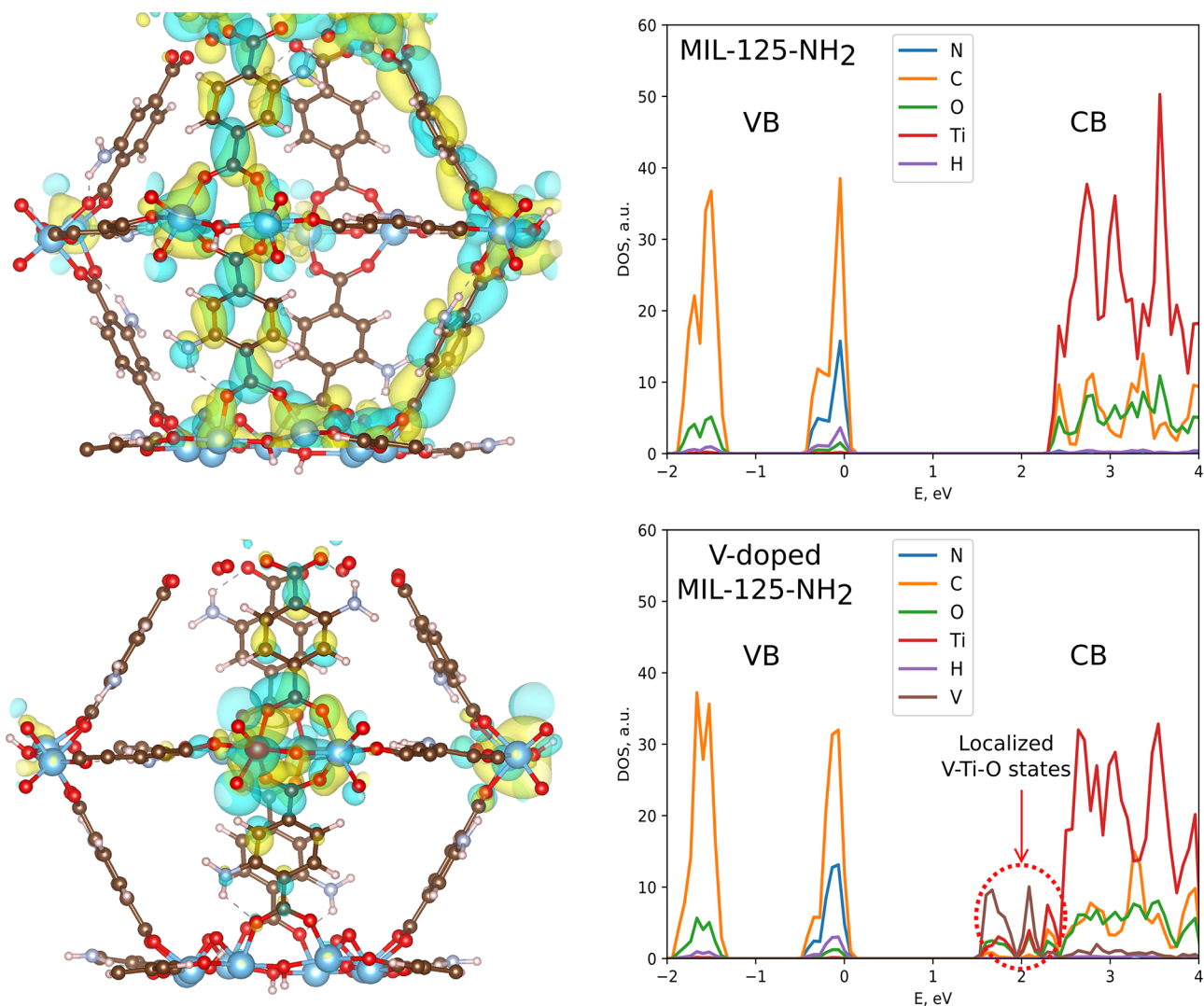
Figure 4. Localized states at the bottom of the conduction band of MIL-125-NH$_2$ generated by V-doping of MIL-125-NH$_2$ (2 Ti sites out of 16 total are occupied by V^{5+}).
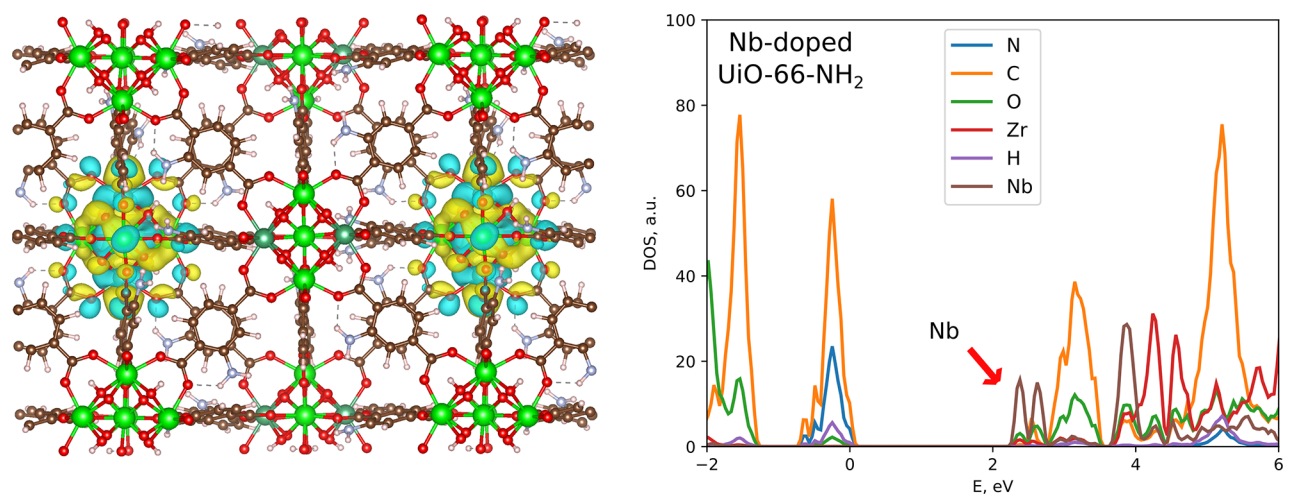
Figure 5. Electron trap states at the bottom of the conduction band of Nb-doped UiO-66-NH$_2$.

concentration (SI, Figure S1). Already this amount of V decreases the CB edge position toward −4.5 eV, and a further concentration increase toward 1/4 shifts CB to −4.8 eV. However, in terms of absolute energy level alignment it should

be born in mind that the electrostatic potential at the center of a pore does not necessarily coincide with the vacuum potential far away from the MOF surface; moreover, these values do not include temperature effect, so the absolute values should be
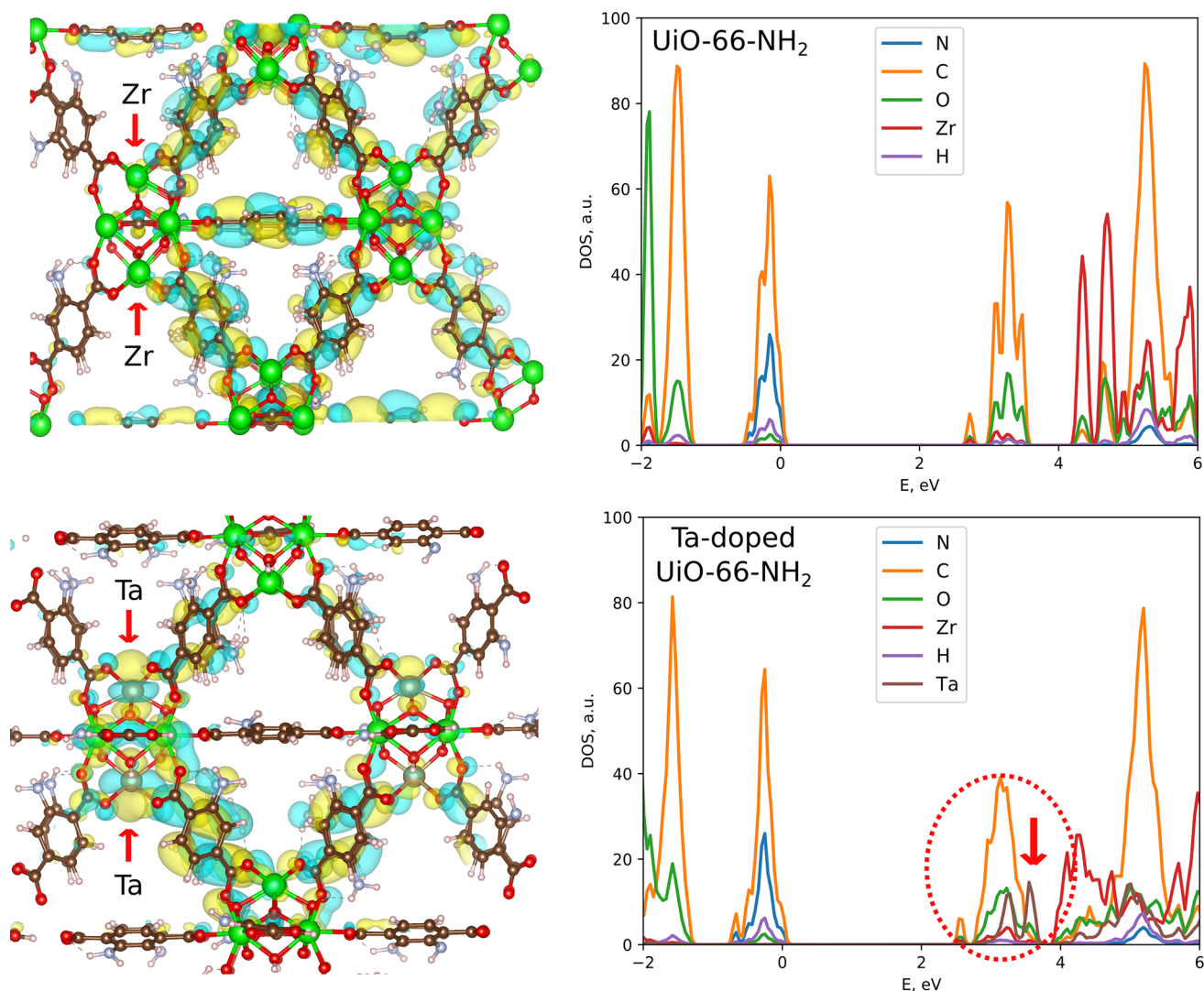
Figure 6. Enhancing metal−ligand hybridization via Ta-doping of UiO-66. 25% of Zr is substituted by Ta, placing 2 Ta per node in 3 out of 4 nodes.

considered as indicative of band positions. The V concentration dependence of the band gap is shown in Figure S2.

W and Nb are lowering the CB edge of MIL-125-NH$_2$. Nb improves the localization on the node, although, as it can be seen from the density of states, C atoms of ligands, as well as Ti, still contribute to the LUCO state (Figure S3, Supporting Information). The Nb$_2$O$_5$ band gap is 0.2 eV higher than that of TiO$_2$,[35] which correlates with a moderate increase in the localization. Regarding WO$_3$, despite the fact that it has much higher electron affinity than TiO$_2$,[35] both Ti and W states contribute to the bottom of the conduction band, suggesting that this criterion alone does not guarantee the localization solely on the dopant metal. The observed moderate decrease of CB position is in line with the optical band gap lowering in W-doped TiO$_2$.[39]

Replacement of Ti by Sn does not enhance LUCO localization, as Sn states lie above those of Ti; moreover the CB position is slightly shifted upward in energy. This example illustrates that solely the alignment criterion is not sufficient for prediction of trap formation. Indeed, SnO$_2$ has a 0.3 eV larger band gap than TiO$_2$.[35]

Regarding UiO-66-NH$_2$, incorporation of Nb results in shallow trap states overlapping with the conduction band edge

(Figure 5) and overall concentration-dependent shift of the CB relative to pure UiO-66-NH$_2$. The Nb concentration dependence of the band gap is illustrated in Figure S2.

We also explore the effect of W substitution in UiO-66-NH$_2$. In that case, W generates deep trap states in the band gap, substantially reducing its width and mainly localized on W and neighboring O atoms.

Ta-doping shifts down the metal states (Figure 6), closing the gap between Zr-centered levels and the bottom of the conduction band, formed by the ligand orbitals. The LUCO in this case stays centered on the ligand. This example demonstrates that the electron affinity of the dopant can be insufficient to create the metal states below the ligand ones. Meanwhile, it shows how doping can be used to close the energy gap between different zones of the MOF conduction band. Such a closing should *a priori* facilitate the relaxation of an excited hot electron toward the bottom of the conduction band. Thus, in the case of UiO-66 Ta can be used as a co-dopant with another metal. Moreover, increased metal−ligand delocalization, ensured by Ta, is *a priori* favorable for enhancing the excited state conductivity, which is essential for photovoltaic applications and whose amplitude can be modulated through the dopant concentration change.

Partial substitution of Y into UiO-66-NH$_2$, accompanied by hydroxylation of bridging oxygen atoms, creates Y states well above the conduction band edge. This is an expected result considering the absolute CB position of Y$_2$O$_3$ situated ca. 1.0−2.0 eV above that of ZrO$_2$. Therefore, the band gap, which is similar in the case of Y$_2$O$_3$ and ZrO$_2$, cannot be used as the sole criterion for dopant selection.

The summary of band alignment and band gap parameters for doped MIL-125-NH$_2$ and UiO-66-NH$_2$ is presented in Figure 7.
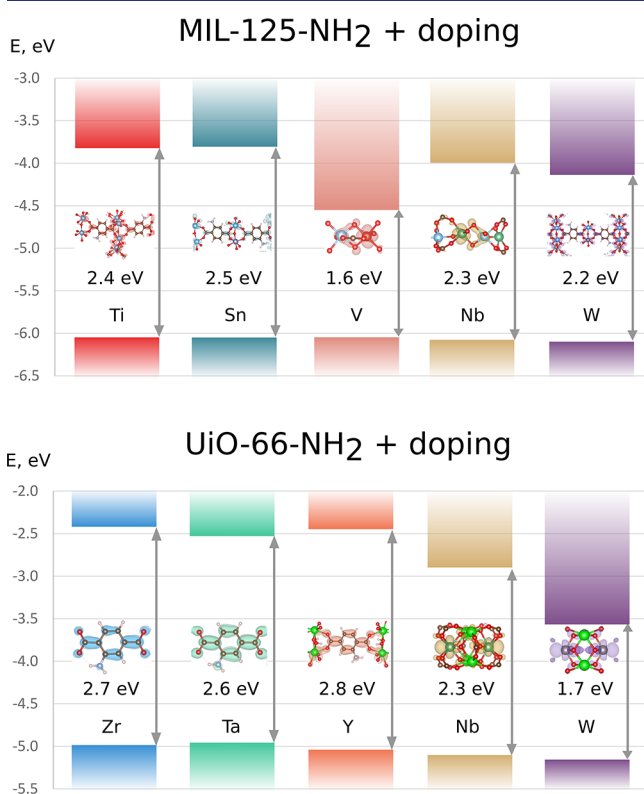
Figure 7. Band alignment in doped MIL-125-NH$_2$ and UiO-66-NH$_2$. Ti and Zr correspond to undoped compounds. Dopant concentrations in MIL-125-NH$_2$: Sn,Nb,W- 4/16; V- 2/16. Dopant concentrations in UiO-66-NH$_2$: Y- 4/24; Ta,Nb- 6/24; W- 2/24.

To validate this approach, in the next section we confirm experimentally the possibility to tune the absorption spectrum, in particular, absorption onset, which is indicative of band gap change and conduction band energy alignment shift, in pristine MIL-125-NH$_2$ and UiO-66-NH$_2$ by V and Nb doping, respectively.

■ EXPERIMENTAL VALIDATION

This work relies on the synthetic feasibility of metal replacement. Although there are various reports in the literature of synthetic procedures[40] and postsynthetic modifications,[41] a particularly challenging system is doping with metal ions in the 5+ oxidation state.[42] Until recently, most MOFs were synthesized using divalent ions of 3d transition metals. Higher valence metals are rare due to the high reactivity of these 4+ and 5+ metal cations forming oxides or poorly crystalline coordination polymers.[43] Examples include Ta^{5+}-based MOF[44] and external V^{5+} node functionalization.[45] Incorporation of Nb$_2$O$_5$ oxide clusters is also reported as an external MOF functionalization,[46] and Nb^{5+} is known in the inorganic pillars NbOF$_5^{2-}$ of the KAUST-7 framework,[47] indicating that the Nb^{5+} oxidation state is not incompatible with the organic MOF environment.

To validate our doping strategy experimentally, we explore the possibility to tune the electronic properties of pristine MIL-125-NH$_2$ and UiO-66-NH$_2$ by V- and Nb-doping, respectively. Both MIL-125-NH$_2$ and UiO-66-NH$_2$ are synthesized as a crystalline powder, with the structure of MIL-125 and UiO-66 solved by Rietveld refinement of the powder X-ray pattern (PXRD).[48,49] By doping MIL-125-NH$_2$ with V, and UiO-66-NH$_2$ with Nb, the predicted electronic structure would lead to a color change due to the shift in the absorption edge of the material. Evidence that doped material has retained the MIL-125 PXRD, while demonstrating a red shift in the absorption edge, would be a powerful indication that V and Nb have been incorporated into MIL-125-NH$_2$ and UiO-66-NH$_2$, respectively.

A synthesis of V-doped MIL-125-NH$_2$ with 12.5% and 25% doping is performed, utilizing the appropriate ratio of metal salts in the synthesis; detailed information about the synthesis and characterization is given in the SI. Inductively coupled plasma optical emission spectrometry (ICP-OES) analysis of the resulting material shows a %V content close to that of the reagent ratio (Table S4, SI), indicating that the V is indeed
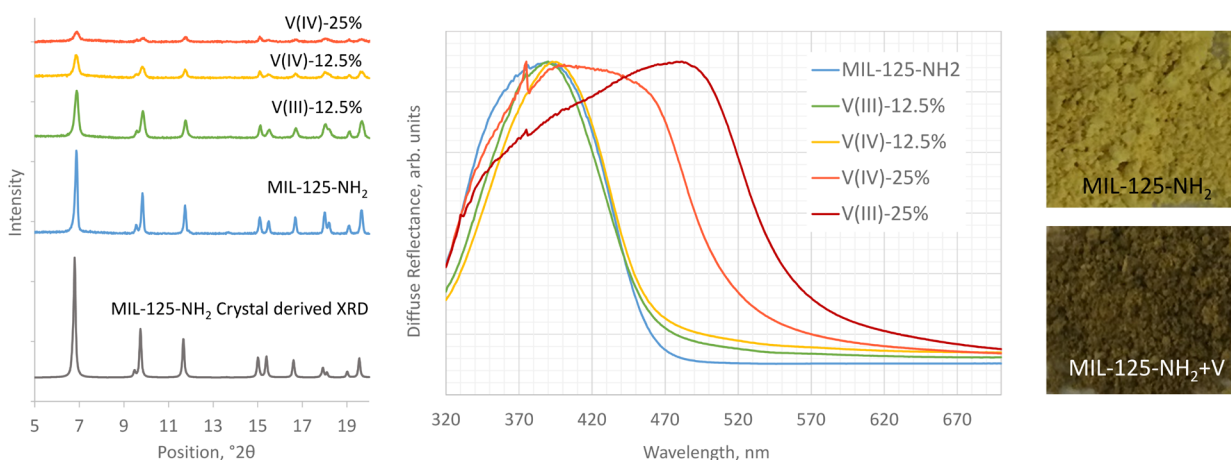
Figure 8. V-doped MIL-125-NH$_2$ samples: XRD patterns, UV/vis spectra, and photos of powders.
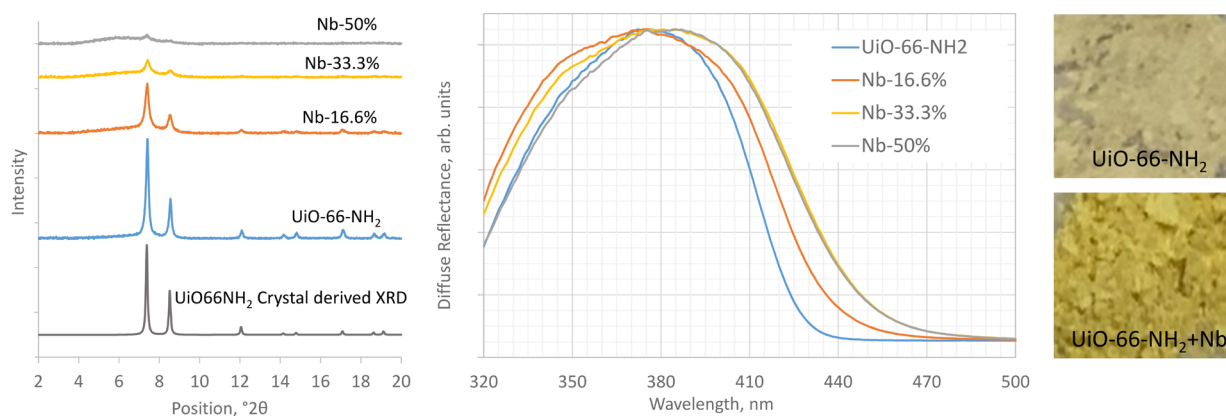
Figure 9. Nb-doped UiO-66-NH$_2$ samples: XRD patterns, UV/vis spectra, and photos of powders.

present in the material. With titanium present in a Ti8 cluster in pristine MIL-125-NH$_2$, the ratio of V:Ti lies close to the expected 1:7 and 2:6 ratios (Table S4). The XRD patterns, UV/vis absorption spectra, and images of the powders are shown in Figure 8. Incorporation of V, as expected, substantially red shifts the absorption onset, in line with the theoretically observed appearance of the V states at the bottom of the conduction band. This shift is evident from the dramatic color change of the powder of pristine MIL-125-NH$_2$ (yellow) compared to the doped material (brown). Ideally, single-crystal analysis could confirm the incorporation of V; however, like the pristine material, the doped material does not form sufficiently large crystals. Therefore, our analysis is based on powder XRD and optical spectra. The XRD confirms the MIL-125-NH$_2$ structure is retained; as the concentration of V is increased, we observe a decreasing intensity and broadening of the peaks. This indicates that the crystallinity decreases with increasing concentration of V. The reactive Ti^{4+} precursor rapidly reacts with ligand to form the MOF structure, and this limits the controlled addition of the V into the structure that would permit long-range crystalline material. However, our calculations predict a relatively large shift (ca. 100 nm, Figures 7, S2) of the absorption onset upon doping with V, which nicely corresponds to the experimental spectral figures, giving a strong indication that V has been incorporated into the Ti oxide cluster.

Figure 9 shows the results of the synthesis of Nb-doped UiO-66-NH$_2$ with 16.6%, 33.3%, and 50% Nb concentrations. As with the V-doped MIL-125-NH$_2$ synthesis, the doping was performed by using the appropriate ratio of metal salts in the synthesis. ICP-OES analysis shows the presence of Nb in the material, the %Nb being akin to that used in the synthesis. UiO-66-NH$_2$ has a Zr6-based oxide cluster as the metal node, in which on average 1, 2, or 3 Zr ions are replaced with Nb (Table S5). The photos of the powders already show that the effect of Nb on the color is less dramatic, compared to V in MIL-125-NH$_2$. Also for this material we have to rely on the powder XRD analysis to confirm the UiO-66 structure. The 16.6% Nb-doped sample retains an almost identical X-ray pattern to the undoped UiO-66-NH$_2$. Increasing Nb concentration lowers the crystallinity of the material, as evidenced from the peak broadening and lower intensity of the higher angle peaks in the PXRD pattern.

Our calculations predict a downward shift of approximately 0.1−0.4 eV (Figures 7, S2) of conduction band position due to the appearance of Nb states at the CB edge, which again nicely

corresponds to the data in Figure 9. Indeed, for the 16.6% Nb-doped sample we observe a deeper yellow compared to the pristine material and also adsorption edge red shifting. Increasing the Nb concentration red shifts the absorption edge further. Nb$_2$O$_5$ has a band gap of 3.4 eV;[35] thus its formation as an alternative product cannot induce an absorption red shift for the Nb-doped sample. This evidence gives a strong suggestion that we have incorporated Nb into the UiO-66-NH$_2$ framework.

Interestingly, Nb-containing MOFs are relatively rare. Eddaoudi and co-workers[47] were among the first to perform a synthesis incorporating Nb^{5+} into a framework, in which Nb-based pillars were connecting 2D layers. Here, we have compelling evidence that Nb can also be incorporated into the full 3D framework. Importantly, this synthesis, performed in a one-pot approach, also confirms that heterovalent metals can occupy Zr positions in UiO-66 topology, providing the routes for rational design of MOFs with targeted electronic structure.

CONCLUSIONS

In summary, doping of metal nodes in metal−organic frameworks is an efficient strategy to modify the band gap and band edge position, as well as to achieve metal-centered electron localization and alternate the degree of ligand−metal hybridization. Oxide band alignment and band gap are useful criteria for prescreening of dopants. In particular, to achieve an efficient charge separation via creation of metal-centered electron traps, the dopant metal should form a more reducible metal oxide than the host metal, which translates into a smaller band gap and lower absolute position of the conduction band edge. In general, following these criteria allows achieving a favorable change of electronic structure in all cases where the energy level alignment is a decisive factor. The possibility to use these rules for targeted design of MOFs with predefined electronic structure features was experimentally demonstrated for UiO-66-NH$_2$(Zr,Nb) and MIL-125-NH$_2$(Ti,V) systems. The described general principles are applicable for any MOF architecture and can be used to fine-tune the electronic properties of existing MOFs in a targeted way.

ASSOCIATED CONTENT

Ⓢ Supporting Information

The Supporting Information is available free of charge on the ACS Publications website at DOI: 10.1021/jacs.8b13667.

Computational details, experimental section, localization indices, computed concentration dependence of the

band gaps, densities of states of doped MIL-125-NH$_2$ and UiO-66-NH$_2$, dopant selection criteria based on reducibility of metal oxides, elemental analysis, ICP-OES results, thermogravimetric analysis (PDF)

■ AUTHOR INFORMATION

Corresponding Author

*olga.syzgantseva@epfl.ch

ORCID ⊙

Berend Smit: 0000-0003-4653-8562

Olga A. Syzgantseva: 0000-0002-0270-4621

Notes

The authors declare no competing financial interest.

■ REFERENCES

(1) Zhou, H.-C.; Long, J. R.; Yaghi, O. M. Introduction to Metal-Organic Frameworks. *Chem. Rev.* **2012**, *112*, 673−674.

(2) Eddaoudi, M.; Moler, D. B.; Li, H.; Chen, B.; Reineke, T. M.; O'Keeffe, M.; Yaghi, O. M. Modular Chemistry: Secondary Building Units as a Basis for the Design of Highly Porous and Robust Metal-Organic Carboxylate Frameworks. *Acc. Chem. Res.* **2001**, *34*, 319−330.

(3) Furukawa, H.; Cordova, K. E.; O'Keeffe, M.; Yaghi, O. M. The Chemistry and Applications of Metal-Organic Frameworks. *Science* **2013**, *341*, 1230444.

(4) Simon, C. M.; Kim, J.; Gomez-Gualdron, D. A.; Camp, J. S.; Chung, Y. G.; Martin, R. L.; Mercado, R.; Deem, M. W.; Gunter, D.; Haranczyk, M.; Sholl, D. S.; Snurr, R. Q.; Smit, B. The materials genome in action: identifying the performance limits for methane storage. *Energy Environ. Sci.* **2015**, *8*, 1190−1199.

(5) Boyd, P. G.; Lee, Y.; Smit, B. Computational development of the nanoporous materials genome. *Nature Reviews Materials* **2017**, *2*, 17037.

(6) Lee, K.; Howe, J. D.; Lin, L.-C.; Smit, B.; Neaton, J. B. Small-Molecule Adsorption in Open-Site Metal-Organic Frameworks: A Systematic Density Functional Theory Study for Rational Design. *Chem. Mater.* **2015**, *27*, 668−678.

(7) Planas, N.; Dzubak, A. L.; Poloni, R.; Lin, L.-C.; McManus, A.; McDonald, T. M.; Neaton, J. B.; Long, J. R.; Smit, B.; Gagliardi, L. The Mechanism of Carbon Dioxide Adsorption in an Alkylamine-Functionalized Metal-Organic Framework. *J. Am. Chem. Soc.* **2013**, *135*, 7402−7405.

(8) Trousselet, F.; Archereau, A.; Boutin, A.; Coudert, F.-X. Heterometallic Metal-Organic Frameworks of MOF-5 and UiO-66 Families: Insight from Computational Chemistry. *J. Phys. Chem. C* **2016**, *120*, 24885−24894.

(9) Bloch, E. D.; Hudson, M. R.; Mason, J. A.; Chavan, S.; Crocellà, V.; Howe, J. D.; Lee, K.; Dzubak, A. L.; Queen, W. L.; Zadrozny, J. M.; Geier, S. J.; Lin, L.-C.; Gagliardi, L.; Smit, B.; Neaton, J. B.; Bordiga, S.; Brown, C. M.; Long, J. R. Reversible CO Binding Enables Tunable CO/H2 and CO/N2 Separations in Metal-Organic Frameworks with Exposed Divalent Metal Cations. *J. Am. Chem. Soc.* **2014**, *136*, 10752−10761.

(10) Liu, B.; Yang, Q.; Xue, C.; Zhong, C.; Chen, B.; Smit, B. Enhanced adsorption selectivity of hydrogen/methane mixtures in metal-organic frameworks with interpenetration: A molecular simulation study. *J. Phys. Chem. C* **2008**, *112*, 9854−9860.

(11) Poloni, R.; Lee, K.; Berger, R.; Smit, B.; Neaton, J. Understanding trends in CO$_2$ adsorption in metal-organic frameworks with open-metal sites. *J. Phys. Chem. Lett.* **2014**, *5*, 861−865.

(12) Witman, M.; Ling, S.; Anderson, S.; Tong, L.; Stylianou, K.; Slater, B.; Smit, B.; Haranczyk, M. In silico design and screening of hypothetical MOF-74 analogs and their experimental synthesis. *Chemical Science* **2016**, *7*, 6263−6272.

(13) Simon, C.; Mercado, R.; Schnell, S.; Smit, B.; Haranczyk, M. What Are the Best Materials to Separate a Xenon/Krypton Mixture? *Chem. Mater.* **2015**, *27*, 4459−4475.

(14) Hendon, C. H.; Rieth, A. J.; Korzyński, M. D.; Dincă, M. Grand Challenges and Future Opportunities for Metal-Organic Frameworks. *ACS Cent. Sci.* **2017**, *3*, 554−563.

(15) Wang, W.; Xu, X.; Zhou, W.; Shao, Z. Recent Progress in Metal-Organic Frameworks for Applications in Electrocatalytic and Photocatalytic Water Splitting. *Adv. Sci.* **2017**, *4*, 1600371.

(16) Chen, Y.; Wang, D.; Deng, X.; Li, Z. Metal-organic frameworks (MOFs) for photocatalytic CO2 reduction. *Catal. Sci. Technol.* **2017**, *7*, 4893−4904.

(17) Xu, H.-Q.; Hu, J.; Wang, D.; Li, Z.; Zhang, Q.; Luo, Y.; Yu, S.-H.; Jiang, H.-L. Visible-Light Photoreduction of CO2 in a Metal-Organic Framework: Boosting Electron-Hole Separation via Electron Trap States. *J. Am. Chem. Soc.* **2015**, *137*, 13440−13443.

(18) Allendorf, M. D.; Bauer, C. A.; Bhakta, R. K.; Houk, R. J. T. Luminescent metal-organic frameworks. *Chem. Soc. Rev.* **2009**, *38*, 1330−1352.

(19) Wang, L. J.; Deng, H.; Furukawa, H.; Gándara, F.; Cordova, K. E.; Peri, D.; Yaghi, O. M. Synthesis and Characterization of Metal-Organic Framework-74 Containing 2, 4, 6, 8, and 10 Different Metals. *Inorg. Chem.* **2014**, *53*, 5881−5883.

(20) Yoon, J. W.; Seo, Y.-K.; Hwang, Y. K.; Chang, J.-S.; Leclerc, H.; Wuttke, S.; Bazin, P.; Vimont, A.; Daturi, M.; Bloch, E.; Llewellyn, P. L.; Serre, C.; Horcajada, P.; Grenèche, J.-M.; Rodrigues, A. E.; Férey, G. Controlled Reducibility of a Metal-Organic Framework with Coordinatively Unsaturated Sites for Preferential Gas Sorption. *Angew. Chem., Int. Ed.* **2010**, *49*, 5949−5952.

(21) Xie, L. S.; Sun, L.; Wan, R.; Park, S. S.; DeGayner, J. A.; Hendon, C. H.; Dincă, M. Tunable Mixed-Valence Doping toward Record Electrical Conductivity in a Three-Dimensional Metal-Organic Framework. *J. Am. Chem. Soc.* **2018**, *140*, 7411−7414.

(22) Sun, D.; Sun, F.; Deng, X.; Li, Z. Mixed-Metal Strategy on Metal-Organic Frameworks (MOFs) for Functionalities Expansion: Co Substitution Induces Aerobic Oxidation of Cyclohexene over Inactive Ni-MOF-74. *Inorg. Chem.* **2015**, *54*, 8639−8643.

(23) Brozek, C. K.; Dincă, M. Ti^{3+}-, V$^{2+/3+}$-, Cr$^{2+/3+}$-, Mn^{2+}-, and Fe^{2+}-Substituted MOF-5 and Redox Reactivity in Cr- and Fe-MOF-5. *J. Am. Chem. Soc.* **2013**, *135*, 12886−12891.

(24) Botas, J. A.; Calleja, G.; Sánchez-Sánchez, M.; Orcajo, M. G. Cobalt Doping of the MOF-5 Framework and Its Effect on Gas-Adsorption Properties. *Langmuir* **2010**, *26*, 5300−5303.

(25) Hendrickx, K.; Joos, J. J.; De Vos, A.; Poelman, D.; Smet, P. F.; Van Speybroeck, V.; Van Der Voort, P.; Lejaeghere, K. Exploring Lanthanide Doping in UiO-66: A Combined Experimental and Computational Study of the Electronic Structure. *Inorg. Chem.* **2018**, *57*, 5463−5474.

(26) Wu, X.-P.; Gagliardi, L.; Truhlar, D. G. Cerium Metal-Organic Framework for Photocatalysis. *J. Am. Chem. Soc.* **2018**, *140*, 7904−7912.

(27) Santiago Portillo, A.; Baldoví, H. G.; García Fernandez, M. T.; Navalón, S.; Atienzar, P.; Ferrer, B.; Alvaro, M.; Garcia, H.; Li, Z. Ti as Mediator in the Photoinduced Electron Transfer of Mixed-Metal NH2-UiO-66(Zr/Ti): Transient Absorption Spectroscopy Study and Application in Photovoltaic Cell. *J. Phys. Chem. C* **2017**, *121*, 7015−7024.

(28) Yue, Z.; Liu, S.; Liu, Y. Yttria stabilized zirconia derived from metal-organic frameworks. *RSC Adv.* **2015**, *5*, 10619−10622.

(29) Castells-Gil, J.; Padial, N. M.; Almora-Barrios, N.; Albero, J.; Ruiz-Salvador, A. R.; González-Platas, J.; García, H.; Martí-Gastaldo, C. Chemical Engineering of Photoactivity in Heterometallic Titanium-Organic Frameworks by Metal Doping. *Angew. Chem., Int. Ed.* **2018**, *57*, 8453−8457.

(30) Nasalevich, M. A.; Hendon, C. H.; Santaclara, J. G.; Svane, K.; van der Linden, B.; Veber, S. L.; Fedin, M. V.; Houtepen, A. J.; van der Veen, M. A.; Kapteijn, F.; Walsh, A.; Gascon, J. Electronic origins of photocatalytic activity in d0 metal organic frameworks. *Sci. Rep.* **2016**, *6*, 23676.

(31) Nasalevich, M. A.; Goesten, M. G.; Savenije, T. J.; Kapteijn, F.; Gascon, J. Enhancing optical absorption of metal-organic frameworks for improved visible light photocatalysis. *Chem. Commun.* **2013**, *49*, 10575−10577.

(32) Pu, S.; Xu, L.; Sun, L.; Du, H. Tuning the optical properties of the zirconium-UiO-66 metal-organic framework for photocatalytic degradation of methyl orange. *Inorg. Chem. Commun.* **2015**, *52*, 50−52.

(33) Fu, Y.; Sun, D.; Chen, Y.; Huang, R.; Ding, Z.; Fu, X.; Li, Z. An Amine-Functionalized Titanium Metal-Organic Framework Photocatalyst with Visible-Light-Induced Activity for CO2 Reduction. *Angew. Chem., Int. Ed.* **2012**, *51*, 3364−3367.

(34) Sun, D.; Fu, Y.; Liu, W.; Ye, L.; Wang, D.; Yang, L.; Fu, X.; Li, Z. Studies on Photocatalytic CO2 Reduction over NH2-Uio-66(Zr) and Its Derivatives: Towards a Better Understanding of Photocatalysis on Metal-Organic Frameworks. *Chem. - Eur. J.* **2013**, *19*, 14279−14285.

(35) Xu, Y.; Schoonen, M. A. The absolute energy positions of conduction and valence bands of selected semiconducting minerals. *Am. Mineral.* **2000**, *85*, 543.

(36) Helali, Z.; Jedidi, A.; Syzgantseva, O. A.; Calatayud, M.; Minot, C. Scaling reducibility of metal oxides. *Theor. Chem. Acc.* **2017**, *136*, 100.

(37) Yasin, A. S.; Li, J.; Wu, N.; Musho, T. Study of the inorganic substitution in a functionalized UiO-66 metal-organic framework. *Phys. Chem. Chem. Phys.* **2016**, *18*, 12748−12754.

(38) Krukau, A. V.; Vydrov, O. A.; Izmaylov, A. F.; Scuseria, G. E. Influence of the exchange screening parameter on the performance of screened hybrid functionals. *J. Chem. Phys.* **2006**, *125*, 224106.

(39) Liu, X.; Shi, Y.; Dong, Y.; Li, H.; Xia, Y.; Wang, H. A facile solvothermal approach for the synthesis of novel W-doped TiO2 nanoparticles/reduced graphene oxide composites with enhanced photodegradation performance under visible light irradiation. *New J. Chem.* **2017**, *41*, 13382−13390.

(40) Lammert, M.; Wharmby, M. T.; Smolders, S.; Bueken, B.; Lieb, A.; Lomachenko, K. A.; Vos, D. D.; Stock, N. Cerium-based metal organic frameworks with UiO-66 architecture: synthesis, properties and redox catalytic activity. *Chem. Commun.* **2015**, *51*, 12578−12581.

(41) Sun, D.; Liu, W.; Qiu, M.; Zhang, Y.; Li, Z. Introduction of a mediator for enhancing photocatalytic performance via post-synthetic metal exchange in metal-organic frameworks (MOFs). *Chem. Commun.* **2015**, *51*, 2056−2059.

(42) Leclerc, H.; Devic, T.; Devautour-Vinot, S.; Bazin, P.; Audebrand, N.; Férey, G.; Daturi, M.; Vimont, A.; Clet, G. Influence of the Oxidation State of the Metal Center on the Flexibility and Adsorption Properties of a Porous Metal Organic Framework: MIL-47(V). *J. Phys. Chem. C* **2011**, *115*, 19828−19840.

(43) Assi, H.; Mouchaham, G.; Steunou, N.; Devic, T.; Serre, C. Titanium coordination compounds: from discrete metal complexes to metal-organic frameworks. *Chem. Soc. Rev.* **2017**, *46*, 3431−3452.

(44) Sargazi, G.; Afzali, D.; Mostafavi, A.; Ebrahimipour, S. Y. Ultrasound-assisted facile synthesis of a new tantalum(V) metal-organic framework nanostructure: Design, characterization, systematic study, and CO2 adsorption performance. *J. Solid State Chem.* **2017**, *250*, 32−48.

(45) Nguyen, H. G. T.; Schweitzer, N. M.; Chang, C.-Y.; Drake, T. L.; So, M. C.; Stair, P. C.; Farha, O. K.; Hupp, J. T.; Nguyen, S. T. Vanadium-Node-Functionalized UiO-66: A Thermally Stable MOF-Supported Catalyst for the Gas-Phase Oxidative Dehydrogenation of Cyclohexene. *ACS Catal.* **2014**, *4*, 2496−2500.

(46) Ahn, S.; Thornburg, N. E.; Li, Z.; Wang, T. C.; Gallington, L. C.; Chapman, K. W.; Notestein, J. M.; Hupp, J. T.; Farha, O. K. Stable Metal-Organic Framework-Supported Niobium Catalysts. *Inorg. Chem.* **2016**, *55*, 11954−11961.

(47) Cadiau, A.; Adil, K.; Bhatt, P. M.; Belmabkhout, Y.; Eddaoudi, M. A metal-organic framework−based splitter for separating propylene from propane. *Science* **2016**, *353*, 137−140.

(48) Dan-Hardi, M.; Serre, C.; Frot, T.; Rozes, L.; Maurin, G.; Sanchez, C.; Férey, G. A New Photoactive Crystalline Highly Porous Titanium(IV) Dicarboxylate. *J. Am. Chem. Soc.* **2009**, *131*, 10857−10859.

(49) Valenzano, L.; Civalleri, B.; Chavan, S.; Bordiga, S.; Nilsen, M. H.; Jakobsen, S.; Lillerud, K. P.; Lamberti, C. Disclosing the Complex Structure of UiO-66 Metal Organic Framework: A Synergic Combination of Experiment and Theory. *Chem. Mater.* **2011**, *23*, 1700−1718.